How to cite: Angew. Chem. Int. Ed. 2023, e202312517
doi.org/10.1002/anie.202312517

Biophysics

Isolation and Characterization of Monomeric Human RAD51: A Novel Tool for Investigating Homologous Recombination in Cancer

Francesco Rinaldi[+], Fabrizio Schipani[+], Beatrice Balboni, Federico Catalano, Roberto Marotta, Samuel H. Myers, Viola Previtali, Marina Veronesi, Luigi Scietti, Valentina Cecatiello, Sebastiano Pasqualato, Jose Antonio Ortega, Stefania Girotto[+], and Andrea Cavalli[+]**

Abstract: DNA repair protein RAD51 is a key player in the homologous recombination pathway. Upon DNA damage, RAD51 is transported into the nucleus by BRCA2, where it can repair DNA double-strand breaks. Due to the structural complexity and dynamics, researchers have not yet clarified the mechanistic details of every step of RAD51 recruitment and DNA repair. RAD51 possesses an intrinsic tendency to form oligomeric structures, which make it challenging to conduct biochemical and biophysical investigations. Here, for the first time, we report on the isolation and characterization of a human monomeric RAD51 recombinant form, obtained through a double mutation, which preserves the protein's integrity and functionality. We investigated different buffers to identify the most suitable condition needed to definitively stabilize the monomer. The monomer of human RAD51 provides the community with a unique biological tool for investigating RAD51-mediated homologous recombination, and paves the way for more reliable structural, mechanistic, and drug discovery studies.

[*] F. Rinaldi[+], F. Schipani,[+] B. Balboni, S. H. Myers, V. Previtali, J. A. Ortega, A. Cavalli[+]
Computational and Chemical Biology,
Istituto Italiano di Tecnologia
Via Morego 30, 16163 Genoa (Italy)
E-mail: andrea.cavalli@iit.it

F. Rinaldi[+], B. Balboni, A. Cavalli[+]
Department of Pharmacy and Biotechnology,
University of Bologna
Via Belmeloro 6, 40126 Bologna (Italy)

F. Catalano, R. Marotta
Electron Microscopy Facility, Istituto Italiano di Tecnologia
via Morego 30, 16163 Genoa (Italy)

M. Veronesi, S. Girotto[+]
Structural Biophysics, Istituto Italiano di Tecnologia
via Morego 30, 16163 Genoa (Italy)
E-mail: stefania.girotto@iit.it

L. Scietti, V. Cecatiello, S. Pasqualato
Biochemistry and Structural Biology Unit, Department of Experimental Oncology, IRCCS European Institute of Oncology
Via Adamello 16, 20139 Milan (Italy)

V. Cecatiello, S. Pasqualato
Current address: Structural Biology Research Centre,
Human Technopole Milan
Italy Palazzo Italia Viale Rita Levi-Montalcini 1,
20157 Milan (Italy)

[+] These authors contributed equally to this work.

Introduction

DNA can be subject to various kinds of lesions. Of these, the double-strand break (DSB) is particularly damaging.[1,2] Cells have developed various strategies to repair DSBs. One such strategy is error-free homologous recombination (HR), which plays a critical role in the Synthesis/Growth 2 (S/G2) phases.[2] HR involves several sensor mediators and effectors, of which RAD51 and BRCA2 are critical players.[2,3] Human RAD51 belongs to the RecA/RAD51 family and acts as an ATP-dependent recombinase forming self-assembled oligomeric fibrils, which are crucial to repair damaged DNA.[4,5] Three different interfaces are involved in the interaction among RAD51 protomers within a fibril. The first interface is mediated by ATP, which binds at the interface between two adjacent protomers (Figure S1A). A short β-strand mediates the second interface at the linker region, which binds to a central β-sheet of the ATPase domain of the neighboring protomers (Figure S1B).[4–6] The third interface is an aromatic packing between the Y54 of one protomer and the F195 of another protomer (Figure S1C).[4–6] RAD51 lacks the nuclear localization sequence, and so needs a carrier for transport into the nucleus.[7] BRCA2, a very large protein of 3418 amino acids, transports RAD51 into the nucleus repairing foci.[8–10] BRCA2 interacts with RAD51 across a large region (residues 1002–2085) of BRC repeats (BRC1-8 of 35–40 amino acids each), which display high homology.[8–10] To date, only the interaction of the fourth BRC repeat (BRC4) with RAD51 has been structurally elucidated (Figure S2).[11] This was achieved by

removing the first 97 amino acids of the human orthologue of RAD51 and replacing them with a flexible polypeptide chain linked to BRC4 (an oligopeptide resembling the fourth BRC repeat).[11] Two regions of BRC4 are critical for its interaction with RAD51.[11,12] These are zone I at the N terminal of BRC4, 1524-FX$_1$X$_2$A-1527, and zone II at the C terminal 1545-LFDE-1548 (Figure S2).[11,12] Overall, BRC4 binds to RAD51 through 28 amino acids (1521-1548)[11] (Figure S2). It was recently demonstrated that BRC4 can disassemble RAD51 fibrils in the absence of DNA.[13] This study suggested that, upon DNA damage, BRCA2 (through its BRC repeats) disassembles RAD51 cytosolic fibrils, recruits monomers of RAD51, and transports them into the nucleus.[13]

The oligomeric behavior of RAD51 makes it challenging to investigate this mechanism, allowing for the discovery of only scraps of indirect biochemical evidence of RAD51's interaction with the BRC repeats.[14,15] Disruption of the BRCA2-RAD51 interaction has emerged as a promising strategy for synthetic lethality, including in the combination with PARP inhibitors (PARPi). This approach, dubbed "chemically induced synthetic lethality", opens up new avenues for wider use of PARPi in BRCA2-competent or PARPi-resistant cancer types.[16–19] Indeed, the BRC4-RAD51 interface has been exploited to develop novel protein-protein disruptors.[17–20] Various molecules have been designed to interfere with the binding of BRC4 with RAD51.[17–20] However, in these studies, the oligomeric nature of RAD51 made it challenging to conduct direct biophysical analysis.[14] Hence, there is a clear need to generate a monomeric RAD51 form for biophysical/biochemical investigations. It should be noted that previous attempts have been made to meet this need.[14,21] Pellegrini et al. proposed that the mutation of F86 or A89 with glutamic acid should disrupt the protomer-protomer interaction, thus stabilizing a monomeric RAD51 form.[11,22] Single mutations can reduce RAD51 oligomerization. Still they do not result in a stable monomeric RAD51.[14,22,23] Cell experiments recently demonstrated that only the simultaneous mutation of the two residues severely compromises RAD51 oligomerization and activity.[23] Other attempts have considered the humanization of the archaeal *Pyrococcus furiosus* RadA (*Pf*RadA, 66% similarity with RAD51) leading to the generation of HumRadA22F and HumRadA22 (Figure S3).[21] HumRadA22 has a fully humanized BRC4 binding surface protein while the HumRadA22F has been used to target the FXXA binding pocket to facilitate drug discovery at this site.[20] Scott et al. recently used this chimeric protein to characterize CAM833A, a selective RAD51 inhibitor, which was developed to mimic the FXXA domain of BRC4.[20] HumRadA22, which has high homology with RAD51 including the LFDE domain binding site, has been used to perform biophysical and structural studies with the eight BRC repeats of BRCA2.[24] Indeed, RAD51-RadA chimeras have been relevant tools for biophysical investigations of the BRC repeats-RAD51 interaction and for drug discovery. Nevertheless, this approach has some limitations. First, the chimeric constructs exhibit high homology only at the BRC4 binding sites and lack the flexible N-terminal and L2 domains, potentially affecting folding and limiting the investigations outside the BRC4 repeat binding site. The chimeras may hinder investigations of the interaction of other BRC repeats with RAD51 (e.g. BRC3), which can stabilize the RAD51 N-terminal domain.[25] Indeed, the lack of the N-terminal domain does not allow the investigation of the structural changes that could be induced in this region upon binding of BRC repeats.[26,27]

Herein we describe the isolation of a novel fully human monomeric RAD51 [F86E, A89E] form. We demonstrate the ability of purified monomeric RAD51 (doubly mutated) to bind BRC4 and CAM833A using different and complementary biophysical techniques. The doubly mutated RAD51 monomer preserves both BRC4 binding pockets and the overall protein folding of the wild-type protein. Notably, we assessed different buffer compositions to find the most suitable condition for stabilizing RAD51 monomer in solution. The monomeric RAD51 can be used as a reliable biological tool to carry out biophysical and biochemical assays to characterize the BRCA2-RAD51 interaction and for drug discovery programs that encompass novel hotspot pockets outside of the RAD51-BRC4 interacting surface.

Results and Discussion

The double mutation is not sufficient to stabilize RAD51 monomers

Despite the high propensity of RAD51 to form fibrils, as required for its physiological activity in the presence and absence of DNA, several studies have pursued its isolation and characterization as a monomeric form.[13,21,28] Considering previous studies, we expressed and purified RAD51 harboring both [F86E] and [A89E] mutations (Figure S4). The doubly mutated protein was purified in a buffer in which the oligomeric wild type (WT) form of RAD51 was found to be stable in time, as previously reported.[13] Static Light Scattering (SLS) analyses and size exclusion chromatography (SEC) showed that the mutated RAD51 has an intrinsic tendency to form high molecular weight species similar to the WT form (Figures 1A, 1B and S4). Interestingly, incubating the protein at higher temperature favored RAD51's oligomerization propensity. Fibril morphology, as detected by negative staining transmission electron microscopy (TEM) experiments, allowed a comparison of doubly mutated RAD51 and RAD51 WT samples. The mutated RAD51 forms smaller oligomeric structures than the WT RAD51 (Figure 1C, 1D). A statistical analysis of the mean fibril thickness and length ($n = 100$) showed that the mutated RAD51 has an average thickness of 8 ± 2 nm and an average length of 32 ± 11 nm compared to 14 ± 2 nm (thickness) and 89 ± 33 nm (length) for RAD51 WT (Figure 1C, 1D). All together these findings highlight that the introduction of mutations in the RAD51 oligomerization linker reduces monomer-monomer affinity without completely abolishing this interaction. Interestingly, the mutated protein still displays a tendency to form fibrillary structures bearing a

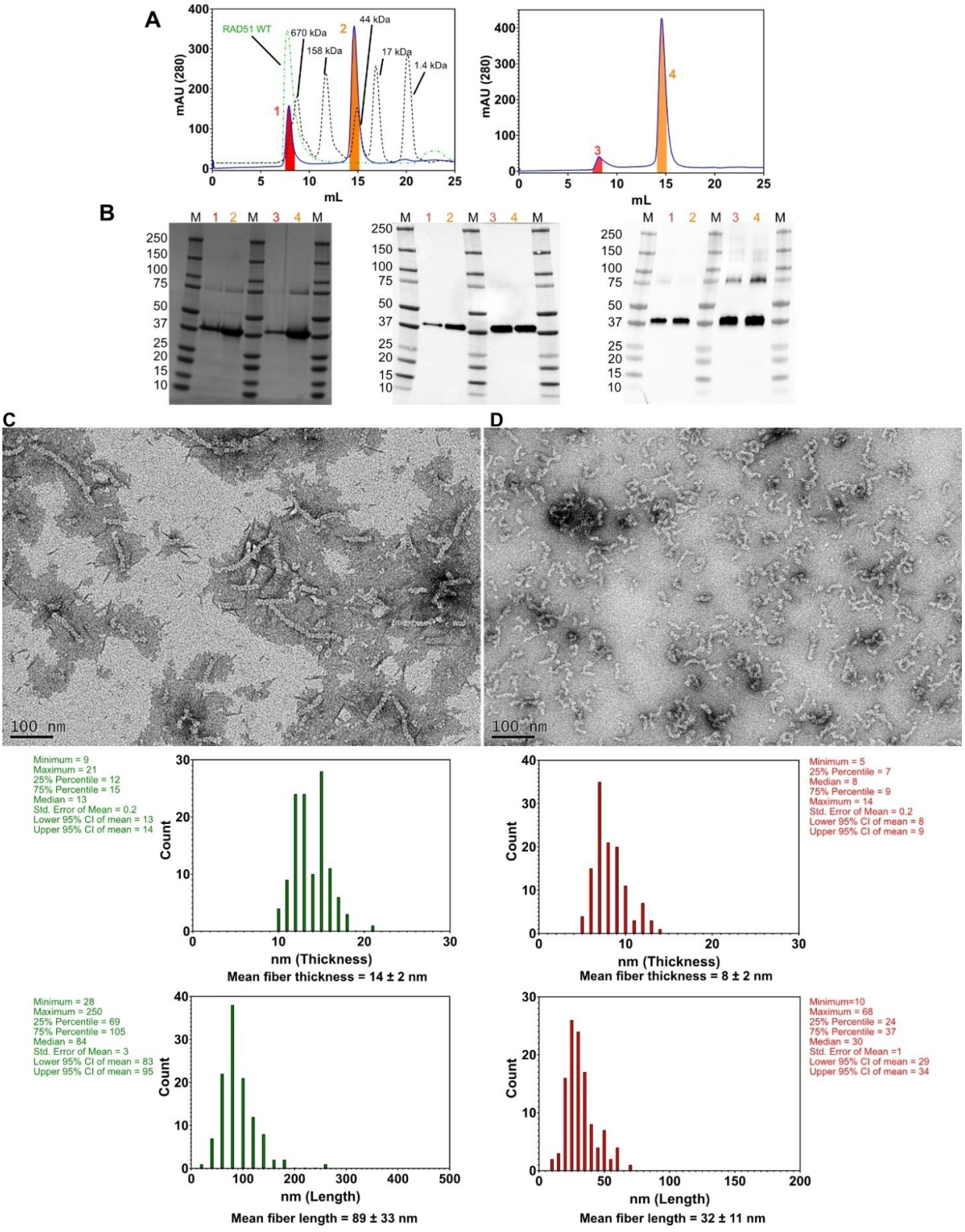

Figure 1. Stability of [F86E, A89E] mutated RAD51 in KCl buffer. A) SEC elution profile (Superdex 200 Increase 10/300 GL) of RAD51 [F86E, A89E]. Left: after 4 hours of incubation at 20 °C. Right: after overnight (O/N) incubation at 4 °C. The dashed and dotted green chromatogram represents the elution profile of RAD51 WT in the same buffer. The black dashed line displays the elution profile of protein calibration markers. The fractions used for SDS Page gel and Western Blot (WB) in (B) are here highlighted in orange and red. B) Left: SDS Page gel Coomassie Blue Staining, Middle: WB Anti-His antibody, Right: WB Anti-RAD51 antibody, M = Marker (Uncropped gels and blots are shown in Figure S48). C) Top: negative staining TEM (NS-TEM) micrograph of RAD51 WT, Bottom: statistical analysis of RAD51 WT fibril thickness and length. D) Top: NS-TEM image of the high molecular weight fractions of RAD51 [F86E, A89E]. Bottom: statistical analysis (frequency distribution) of RAD51 [F86E, A89E] fibril thickness and length.

different morphology compared to RAD51 WT fibrils. Mutated protein instability may be ascribed to a reduction in monomer-monomer affinity, which does not result in a complete abrogation of the interaction. Based on recent biochemical and cellular data provided by Paoletti et al. and Mundia et al. this behaviour was expected for the single mutated [F86E],[22,23] but was unforeseen for the doubly mutated His-RAD51 [F86E, A89E], which was found to abrogate RAD51 fibrillation in cellular experiments.[23]

Sodium sulfate induces RAD51 monomer stabilization

Several studies have reported that buffer composition can influence RAD51's stability and biochemical properties.[29,30] Interestingly, sodium sulfate (Na_2SO_4) inhibits RAD51 ATPase activity and DNA binding.[29,30] Additionally, sulfate anions have been observed in the ATP binding site of two X-ray structures of RAD51 orthologues (*Pf*RadA, *Sc*RAD51), mimicking the ATP/ADP β phosphate (Figure S5).[31,32] This evidence suggested that sulfate anions could interact with RAD51 ATPase domain in a similar manner as ADP, potentially affecting the behavior of both human RAD51 WT and [F86E, A89E] mutated. Considering these observations, we therefore tested the effect of ADP/Mg^{2+} and Na_2SO_4 on RAD51 WT. By performing SEC experiments in a buffer containing KCl and ADP/Mg^{2+} we observed a dissociation of the typical high molecular weight fibrils into smaller species primarily composed of low molecular weight oligomers (Figure 2A). The same effect could be observed by replacing KCl with Na_2SO_4 in absence of co-factors (Figure 2B and S6). These results were corroborated through negative staining TEM experiments which clearly indicated that the presence of ADP/Mg^{2+} or sulfate anions determined the rearrangement of RAD51 fibrils into smaller ring-like species (Figures 2C, 2D). Interestingly, the addition of a peptide resembling BRC4, the BRCA2 repeat showing the highest affinity for RAD51, caused the disruption of RAD51 oligomers in both tested conditions (Figure S6). To further support the hypothesized competition of sulfate anions for the ATP binding site, ATP hydrolysis was evaluated in KCl and Na_2SO_4 buffers by NMR experiments.

As showed in Figure 2E and Table 1, the presence of Na_2SO_4 significantly reduced RAD51 ATP hydrolysis, further supporting the hypothesis of a competition for the same binding site. Having assessed the effect of sulfate anions on RAD51 WT, the behavior and stability of the mutated RAD51 [F86E, A89E] were challenged in the presence of this salt. Strikingly, from SEC and SLS analyses a complete monomeric protein stabilization was achieved by replacing KCl with Na_2SO_4 buffer (Table 2, Figures 3A–E and S7). Interestingly, RAD51 [F86E, A89E] monomer (hereafter named monomeric RAD51) showed a significant reduction in ATP hydrolysis activity compared to RAD51 WT in the same buffer (Figure S7). This was expected since monomerization of RAD51 halves the ATP binding site which is composed by two adjacent ATPase domains.[4–6] RAD51 [F86E, A89E] monomer was further characterized through Circular Dichroism (CD) to assess its secondary structure (Figure 3F). An overlap of the monomeric and WT RAD51 CD spectra allowed to appreciate slight differences in ellipticity, mainly ascribed to helical structure and random coil (others) components (spectra deconvolution analysis in Figure legend 3F), likely linked to the oligomeric state of the WT protein, compared to the monomeric protein. Altogether, our data demonstrated that buffer composition is critical for the stabilization of the recombinant doubly mutated RAD51 to a full monomer. Therefore, such a behavior may be linked to the folding of the ATP binding pocket. Indeed, the presence of ATP/ADP has already been proposed to impact RAD51's structural rearrangements (Figure S8–S10). In particular, the transition from active ATP-bound filament[34] to the inactive ADP-bound form[34] seems to tune the accessibility to one of the BRC4 binding pockets.[6] Moreover, the literature has already reported that sulfate and phosphate ions can stabilize RAD51 by interacting with the ATP binding site.[31,32] These anions may impact on the ATP binding site rearrangement, as they mimic an ADP-bound state, thus stabilizing an inactive RAD51 conformation that is less prone to oligomerization. SEC, TEM and NMR data obtained on RAD51 WT support this hypothesis and provide an explanation for the stability of the doubly mutated RAD51 under this buffer condition. Indeed, as demonstrated by SEC, SLS, CD, NMR, the substitution of KCl with Na_2SO_4 is critical to stabilizing monomeric RAD51. These results suggest that sulfate anions likely induce a rearrangement of the monomeric RAD51 ATPase domain, impairing protein oligomerization.

Table 1: RAD51 ATP hydrolysis in different buffer conditions.

	[ADP] (μM)	Reaction velocity [μM/min]
RAD51 in KCl	243.50 ± 4.95	0.81 ± 0.02
RAD51 in Na_2SO_4	133.50 ± 4.95	0.45 ± 0.02

Table 2: Static Light Scattering analysis of RAD51 [F86E, A89E] in the presence or absence of BRC4 peptide.

	Theoretical Mw	Calculated Mw
RAD51 [F86E, A89E]	39.7 kDa	38.8 kDa
RAD51 [F86E, A89E] -BRC4	43.7 kDa	44.3 kDa

RAD51 monomer binds BRC4, BRC4 FXXA-domain and CAM833A

The interaction of RAD51 monomer with BRC4 was then studied in Na_2SO_4 buffer. Preliminary SLS experiments were performed by incubating monomeric RAD51 in the presence or absence of a 10-fold stoichiometric excess of the BRC4 peptide. Samples incubated with BRC4 eluted at a lower retention volume (higher molecular weight) than RAD51 monomer alone, and the estimated molecular weight confirmed the formation of a 1:1, RAD51:BRC4 complex of ≈44 kDa (Figure 4A and Table 2).

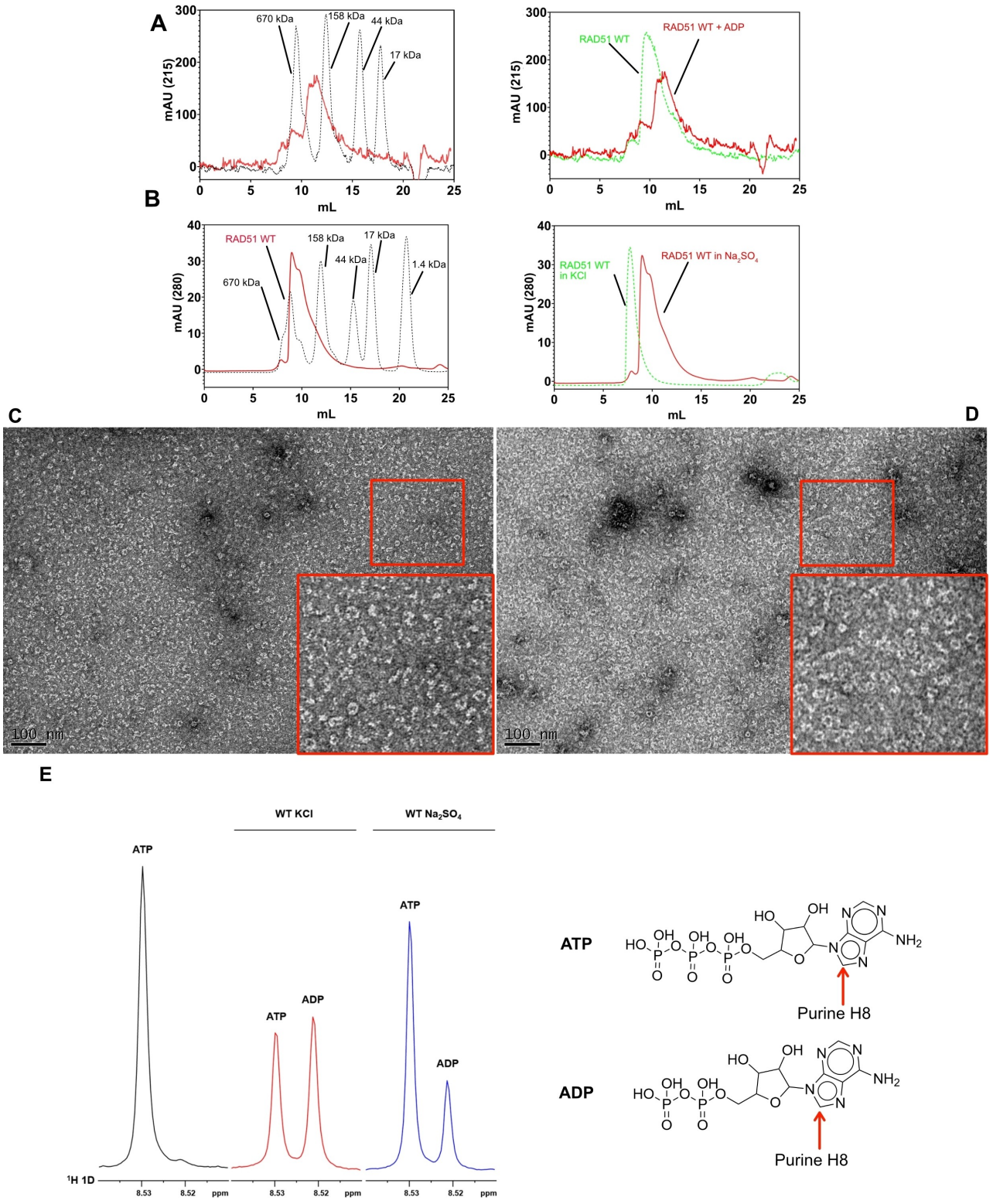

Figure 2. Effect of ADP or Na_2SO_4 buffer on RAD51 WT. A) Left, SEC elution profiles (Superdex 200 Increase 10/300 GL) of RAD51 WT incubated with ADP/$MgCl_2$ in buffer containing KCl and ADP/$MgCl_2$. Right, comparison of elution profiles in the absence (green) or presence (red) of co-factors. B) Left, SEC elution profiles of RAD51 WT in buffer containing Na_2SO_4. Right, comparison of elution profiles in the presence of KCl (green) or Na_2SO_4 (red). The black dashed line outlines the elution profile of protein calibration markers. C) NS-TEM images of RAD51 WT in KCl buffer supplemented with ADP/$MgCl_2$ and D) NS-TEM images of RAD51 WT in Na_2SO_4 buffer. E) Left: ^{1}H 1D NOESY-presat experiments of ATP incubated alone (black) and in the presence of RAD51 WT purified in buffer containing KCl (red) or Na_2SO_4 (blue). Only the ^{1}H signal of purine H8 proton of ATP and ADP are shown. Right: structures of ATP and ADP molecules. The Purine H8 is highlighted with a red arrow.

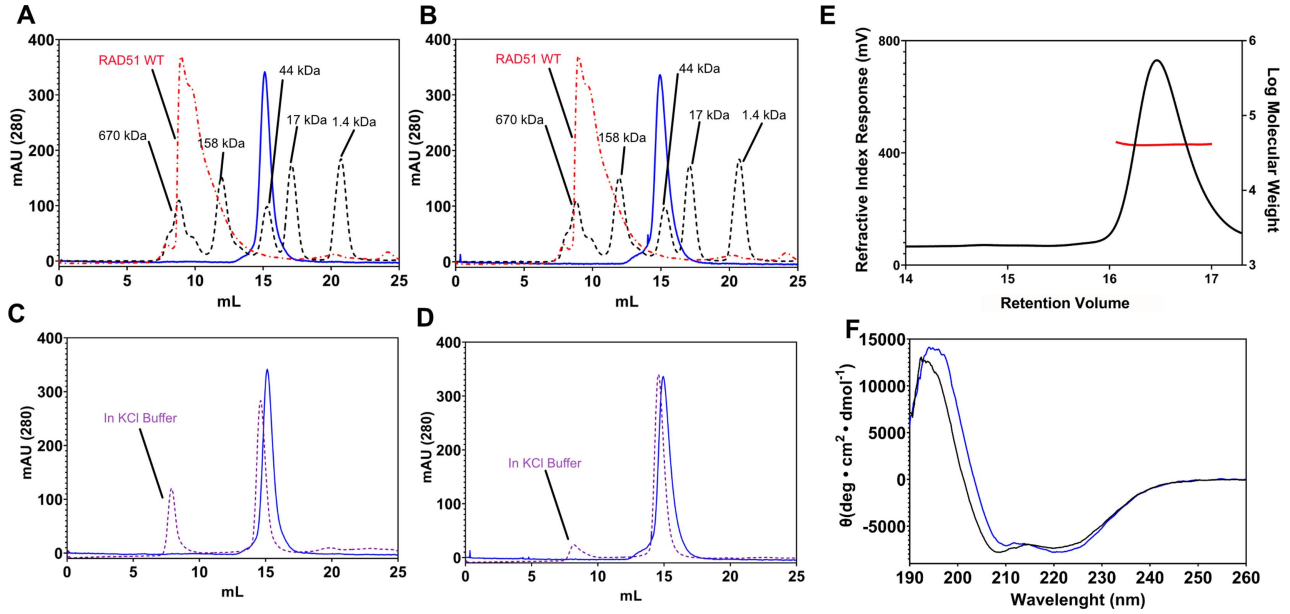

Figure 3. Characterization of RAD51 [F86E, A89E] in Na_2SO_4 buffer. SEC elution profiles (Superdex 200 Increase 10/300 GL). A) After 4 hours of incubation at 20 °C. B) After overnight incubation at 4 °C. Dashed and dotted red line represents the elution of RAD51 WT in buffer containing Na_2SO_4. Dashed black line represent the elution profile of protein calibration markers in the same buffer conditions. Comparison of SEC elution profiles of RAD51 [F86E, A89E] in Na_2SO_4 (continuous blue line) and in KCl buffer (dashed violet line) are reported in (C). After 4 hours of incubation at 20 °C and in (D) after overnight incubation at 4 °C. E) SLS analysis of RAD51 [F86E, A89E] in buffer containing 200 mM Na_2SO_4. F) Overlay of circular dichroism (CD) spectra of RAD51 [F86E, A89E] in black, and RAD51 WT in blue. BeStSel method[33] spectra analysis provided predictions of the secondary structure content for RAD51 [F86E, A89E] (22.6% helix, 10.4% antiparallel β-sheet, 11.0% parallel β-sheet, 15.9% turn and 40.3% others) and for RAD51 WT (24.8% helix, 10.3% antiparallel β-sheet, 11.1% parallel β-sheet, 15.5% turn and 38.3% others). The data are the average of analyses performed on two independent replicates.

The affinity (K_d) of BRC4 for RAD51 monomer was calculated with Microscale Thermophoresis (MST) analysis providing a $K_d \approx 90$ nM (Figure S11A). Fluorescence Polarization (FP) experiments were also performed to corroborate MST results. BRC4 coupled to Fluorescein (hereafter referred to as BRC4*) was titrated against increasing concentrations of RAD51 monomer or RAD51 WT (Figure 4B).[35] The FP-based K_d was ≈20 nM for both RAD51 monomer and RAD51 WT in agreement with MST data. FP competition assays were further set up by titrating a preformed complex of BRC4*-RAD51 Monomer or BRC4*-RAD51 WT with increasing concentrations of unlabeled BRC4 peptide (Figure 4C). A K_d^i of ≈70 nM was obtained for both proteins in agreement with MST data and direct FP assay results (Figure 4C).[35] Thermodynamic characterization of the protein-peptide interaction, performed with Isothermal Titration Calorimetry (ITC) analyses, provided a K_d of ≈40 nM, for the same BRC4-RAD51 interaction (Figures 4D, S11B). Additional experiments were carried out to further corroborate the robustness of the monomeric RAD51. We exploited a fluorinated BRC4-derived peptide containing the FXXA binding motif (a.a. 1521–1532) (Figures 5A, S12), the entire BRC4, and CAM833A (Figure S12), which resembles the FXXA domain, recently designed and characterized by Scott et al. utilizing chimeric HumRadA22F.[20] After we assessed the stability of the fluorinated BRC4-derived peptide in the protein buffer (Figures 5B, S12), we tested its binding to RAD51 monomer in ^{19}F-T_2 filter experiments. The transverse relaxation rate R_2 is a very sensitive parameter due to the large Chemical Shift Anisotropy of ^{19}F nucleus and the large exchange contribution. The response (R_{obs}) in the T_2 filter experiments results in a line broadening of the ^{19}F NMR signal, when binding to the target protein is observed. As shown in Figure 5B, the ^{19}F NMR signal of the ^{19}F-peptide (black) strongly decreases in the presence of protein (red), suggesting that ^{19}F-peptide binds to RAD51 [F86E, A89E] monomer. The binding of the fluorinated peptide to monomeric RAD51 was further corroborated by competitive experiments with BRC4 and CAM833A, two binders of the FXXA domain. As reported in Figure 5B, the signal of fluorinated peptide completely reverts in the presence of the two binders (blue and green), suggesting a complete displacement of the fluorinated peptide, hence competition for the same binding site. After validating the binding of the fluorinated peptide to the RAD51 FXXA domain, we determined an affinity parameter via a rapid and robust competitive NMR assay.[36] Competitive FP experiments were initially performed to determine the affinity of the competitor CAM833A for both RAD51 WT and RAD51 monomer. The affinity of CAM833A for both proteins (K_d) was ≈1–2 μM (Figure 5C). The binding affinity of CAM833A for monomeric RAD51 was also evaluated with ITC, and a K_d of ≈750 nM was calculated in agreement with previous results obtained through HumRadA22F (Figures 5D, S13).[20] These outcomes further confirmed FP data.

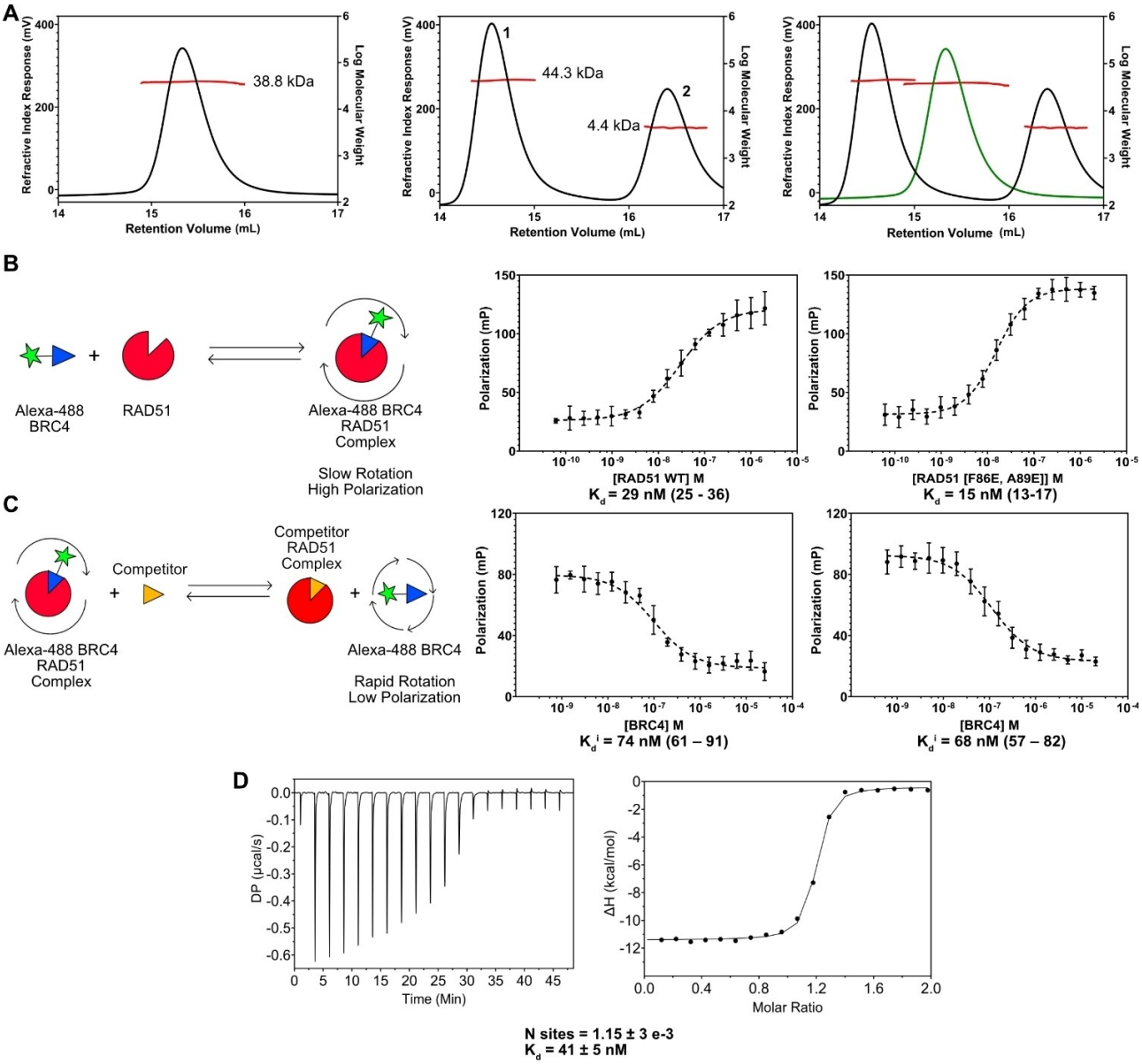

Figure 4. Characterization of the BRC4 interaction with RAD51 [F86E, A89E] Monomer. A) Left: SLS analysis of RAD51 [F86E, A89E] in buffer containing 100 mM Na_2SO_4. Middle: SLS analysis of RAD51 [F86E, A89E] in the same buffer in the presence of BRC4 peptide, peak 1 represents the RAD51-BRC4 complex, peak 2 represents the BRC4 peptide alone. Right: overlay view of the samples in the presence (black) or absence of BRC4 peptide (green). B) Left: schematic representation of fluorescence polarization (FP) assay. Middle: direct FP assay of RAD51 WT with a fixed concentration of labelled BRC4 (BRC4*) (n = 3). Right: direct FP assay of RAD51 [F86E, A89E] with a fixed concentration of BRC4*, (n = 3). C) Left: schematic representation of the competitive FP Assay. Middle: competitive FP assay in which a preformed RAD51 WT-BRC4* complex is titrated with increasing concentrations of unlabeled BRC4 (n = 3). Right: competitive FP assay in which a preformed RAD51 [F86E, A89E] complex is titrated with increasing concentrations of unlabeled BRC4 (n = 3). D) ITC Analysis of the BRC4 - RAD51 [F86E, A89E] interaction.

The affinity of the fluorinated peptide for monomeric RAD51 was successively calculated in NMR experiments using the K_d of BRC4 and CAM833A obtained in ITC experiments. To improve the accuracy of our measurements, the competition experiment was performed in duplicate, using three different concentrations of competitors (1, 2, and 4 µM of BRC4 and 10, 50, and 100 µM of CAM833A, Figure 5E) and calculating the K_d of the ^{19}F-peptide at the three different concentrations for both competitors. The average K_d from the three different concentrations for both competitors is summarized in Table 3. The average K_d of the fluorinated FXXA binding motif peptide for monomeric

Table 3: Average of the K_d summary using both BRC4 and CAM833A as competitors.

Competitor	K_d µM	19^F-pept K_d µM by K_I of competitor
BRC4	0.04	11.5 ± 4.1
CAM833A	0.8	7.8 ± 2.9

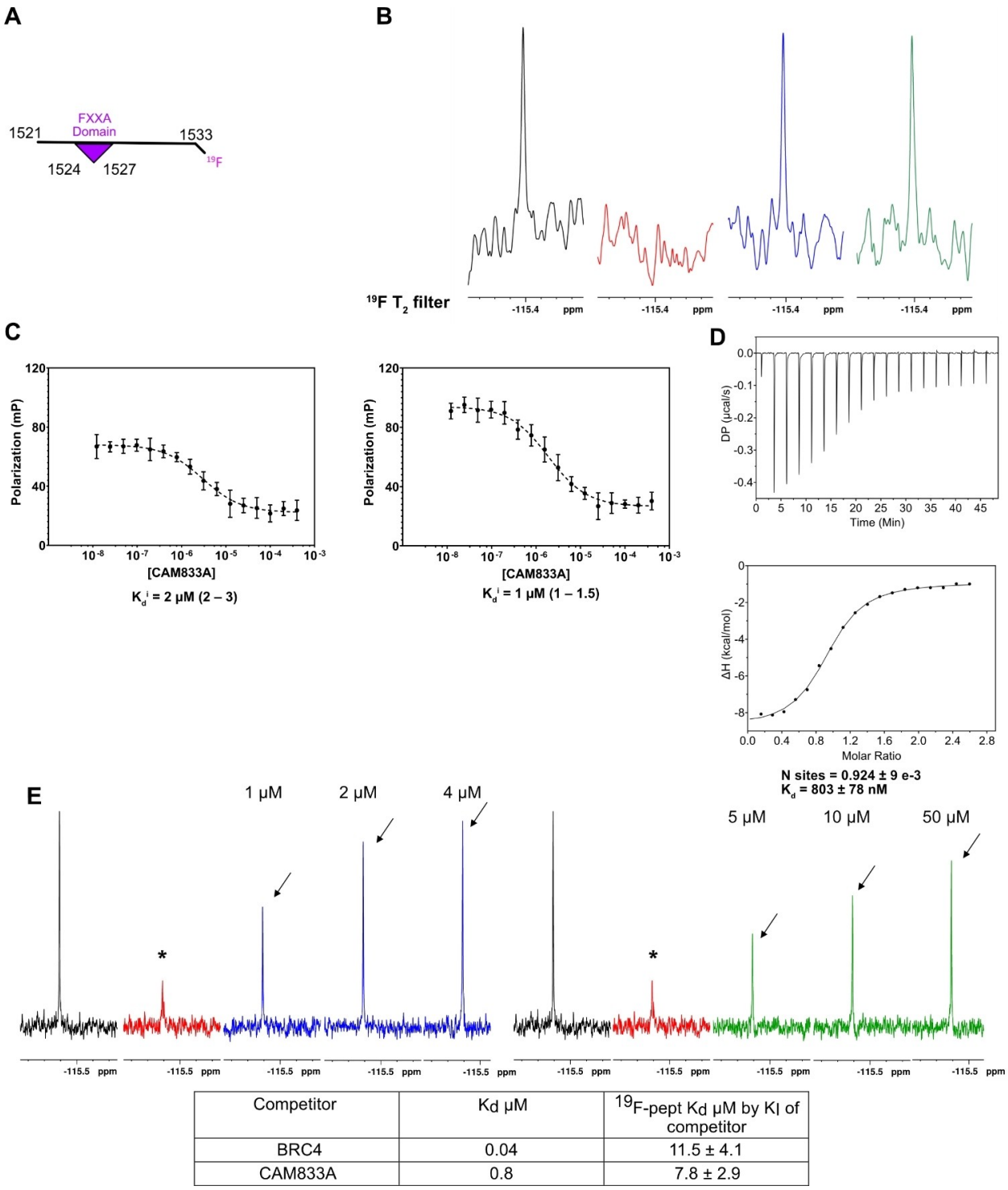

Competitor	Kd μM	^{19}F-pept Kd μM by KI of competitor
BRC4	0.04	11.5 ± 4.1
CAM833A	0.8	7.8 ± 2.9

Figure 5. Characterization of the CAM833A interaction with RAD51 [F86E, A89E] Monomer. A) Left: Schematic representation of Fluorinated FXXA Binding Motif peptide. B) ^{19}F T_2 filter spectra of 20 μM Fluorinated FXXA Binding Motif peptide in the absence (black) and the presence of 1 μM RAD51 [F86E, A89E] (red), or 1 μM RAD51 [F86E, A89E] and 5 μM of BRC4 (blue) or 1 μM RAD51 [F86E, A89E] and 100 μM CAM833A (green). C) Left: Competitive FP Assay in which a preformed RAD51 WT complex is titrated with increasing concentrations of CAM833A (n = 3). Right: Competitive FP Assay in which a preformed RAD51 [F86E, A89E] complex is titrated with increasing concentrations of CAM833A (n = 3). D) ITC Analysis of CAM833A-RAD51 ([F86E, A89E]. E) Left: ^{19}F T_2 filter experiments of ^{19}F-peptide in the absence (black) and presence (red) of RAD51 A89E monomer, RAD51 A89E monomer and 1, 2, and 4 μM BRC4 (blue). Right: ^{19}F T_2 filter experiments ^{19}F-peptide in the absence (black) and presence (red) of RAD51 A89E monomer, and 5, 10, and 50 μM CAM833A (green). The asterisk indicates the line broadening of the peptide's ^{19}F NMR signal in the presence of protein, due to its binding to RAD51 monomer. The arrows indicate a sharpening of the peptide ^{19}F signal due to its displacement from the monomer by BRC4 or CAM833A.

RAD51 was 9.7 ± 3.9 μM. Our data agree with each other and with available data obtained with chimeric and WT proteins, further corroborating the robustness and reliability of the monomeric RAD51.

SAXS studies on monomeric RAD51 and RAD51-BRC4 complex

Finally, to gain novel structural insights into the monomeric RAD51 protein a broad range of crystallization trials were performed. Unfortunately, they did not lead to protein crystals. The monomeric protein was therefore studied by size-exclusion chromatography coupled to small-angle synchrotron X-ray scattering (SEC-SAXS) (Table S1) to better characterize its behavior in solution. SAXS data analysis provided for monomeric RAD51 a molecular weight of 40 kDa and a radius of gyration (R_g) of 30 Å (Table S1, Figure S14). Dimensionless Kratky plot suggested that the RAD51 monomer was folded and possibly flexible, as can be noticed by the shift of the peak-maximum compared to the Guiner-Kratky point (Figure S14).[37–39] This evidence was further supported by calculating the p(r) function through the Indirect Fourier Transformation (IFT). As shown in Figure S14, two features of proteins harboring flexible domains could be appreciated: a smooth decrement to 0 and a large D_{max}.[37] Indeed, the NMR structure of the isolated N-terminal domain of RAD51 (residues 1–114), provided by Aihara and colleagues, showed high mobility of this region when it is not buried in the ATPase domain of a second RAD51 monomer, as most likely happens for the monomeric RAD51 too.[40] SAXS data of monomeric RAD51 were also used to carry out atomistic modeling. Initially, the fitting of a monomer obtained from the X-ray structure of RAD51 filament (PDB ID:5NWL) was attempted with FoXS.[4,41] Nevertheless, a χ^2 value of 41.30 was obtained, suggesting that this model was not representative of the experimental data (Figure S15). Indeed, the 5NWL structure lacks the L2 loop and a large portion at the N-terminal domain, comprising the first 20 amino acids of RAD51, and the 6xHis tag present at the N-terminal in our construct. Additionally, in RAD51 fibrils, the oligomerization linker is buried in the ATPase domain of a second RAD51 monomer and likely blocked in that conformation. This is in contrast to what is observed in the NMR structure of the N-terminal domain of RAD51 alone and, most likely, in the structure of the monomeric full-length protein too.[40] To compensate for the missing regions in the 5NWL model, a complete RAD51 monomer was generated with AlphaFold2 (AF2) (Figures S16, S17).[42,43] Fitting this structure with SAXS data provided a χ^2 of 2.12 in FoXS (Figure S18). This was then used for further studies of the N-terminal domain flexibility.[42,43] Flexibility was assigned to the unstructured regions at the N-terminal domain of RAD51 and modeled through MultiFoXS.[44] The best fit was obtained in a five-state model (Figures 6A–D, S19–S24). Similar results were obtained by removing the first 131 amino acids of RAD51 N-terminal domain and by modeling this region as an unstructured region through the Ensemble Optimization Method (EOM) (Figure S25).[45,46] These data may imply that similar N-terminal domain flexibility could be also observed in the RAD51-BRC4 complex. Indeed, previous evidence, obtained through molecular dynamics simulations,[26] has already suggested that BRC4, upon binding to RAD51, triggers a conformational change at its N-terminal domain. Indeed, this N-terminal unlocking mechanism is in line with BRC4 mechanism of fibrils erosion from their termini that yields to monomeric RAD51.[13] To verify this hypothesis, the His-RAD51—His-BRC4 complex was co-expressed and co-purified to perform SEC-SAXS experiments (Figures S26, S27, and Table S2). Primary data analysis confirmed protein molecular weight and provided a R_g of 34 Å (Table S2). The dimensionless Kratky plot and the p(r) analysis confirmed the typical features of flexible proteins already observed for monomeric RAD51 (Figure S27).[37–39] Therefore, atomistic modeling was performed utilizing the only available high resolution structure of the RAD51-BRC4 complex published by Pellegrini and colleagues in 2001 (PDB entry: 1N0W).[11] Nevertheless, the fitting of this structure yielded a χ^2 value of 179, suggesting that this model was very far from experimental SAXS data (Figure S28). Indeed, the X-ray structure of the complex lacks the first 97 amino-acids of the RAD51 N-terminal domain, the DNA-binding loops L1 and L2 and the His-tags present at the N-terminal portions of both RAD51 and BRC4. An AF model (Figures S29, S30)[42,43] was then generated leading to a significantly improved χ^2 of 10.97 in FoXS (Figure S31), which was however not yet representative of the experimental data. To overcome this issue the RAD51 N-terminal domain, comprising the tag, and the BRC4 His-tag were modeled as disordered regions through EOM (Figures S32, S33),[45,46] confirming that these regions significantly affect the flexibility of the system. In the attempt to eliminate the flexibility ascribable to the tags, SEC-SAXS experiments were performed on RAD51-BRC4 complex deprived of the His-tags (Figures S34, S35 and Table S3). Primary data analysis confirmed a molecular weight of 40 kDa and allowed to calculate a R_g of 29–30 Å (Figure S35, Table S3). Kratky analysis highlighted that the RAD51-BRC4 complex was folded and flexible as also confirmed by the p(r) distribution analysis (Figure S35).[37–39] In analogy with previous experiments, an atomistic modeling was performed. The first trial was carried out utilizing the PDB entry: 1N0W.[11] Despite the fitting of this structure provided a χ^2 value of 76, the removal of tags significantly reduced the discrepancy between the model and the SAXS spectrum (Figure S36 vs Figure S28). To compensate for the missing regions (N-terminal domain, L2 and L1 loop) of the PDB 1N0W an AF model was generated (Figures S37, S38).[42,43] The obtained prediction significantly improved the χ^2 to 9.30 (Figure S39) and was therefore utilized for a multistate modeling (MultiFoXS) of the RAD51 N-terminal domain by assigning flexibility to its unstructured regions.[41,44] The best fits were obtained for three-state, four-state and five-state models which provided a χ^2 of 1.03 (Figures 6E–H and Figures S40–S45). The same χ^2 was obtained by removing the first 98 amino acids of RAD51 at the N-terminal domain and modeling this region as unstructured through EOM (Figures S46, S47).[45,46] Overall, these

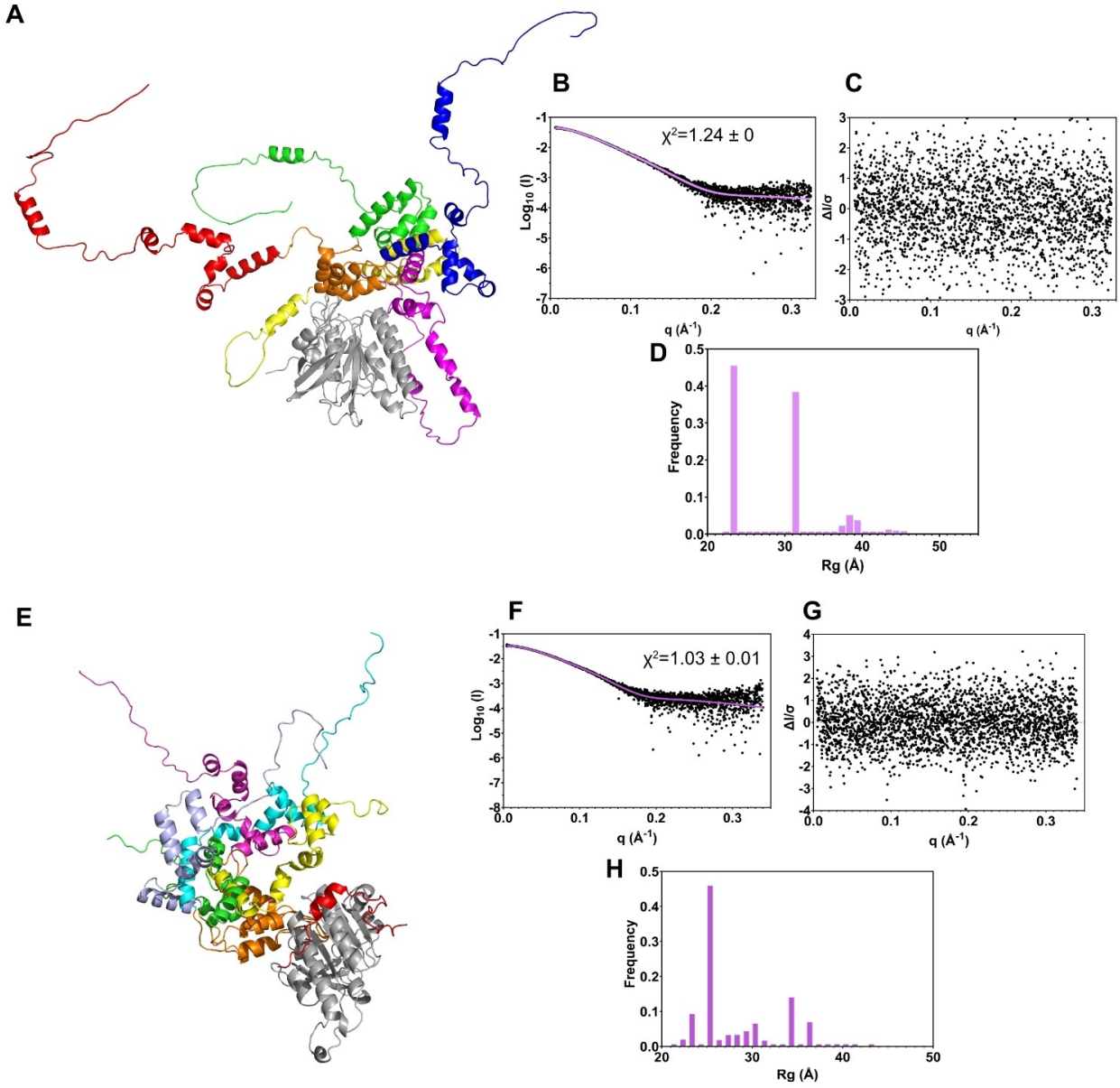

Figure 6. Multi-FoXS modeling [F86E, A89E] RAD51 AF2 predictions in the presence or absence of BRC4 peptide. A) Overlay of the best scoring Multi-FoXS 5-state models for the His-tagged RAD51 monomer. The ATPase domain is in grey, the oligomerization linker in orange and the N-terminal domain in multiple colors. B) Model fit to experimental SAXS data. C) Model residuals. D) Distribution of radii of gyration in the 5-state models. E) Overlay of the best scoring 5-state models for the RAD51-BRC4 complex. The ATPase domain is in grey, the oligomerization linker in orange, and the N-terminal domain in multiple colors. In red the BRC4 peptide. F) Model fit to experimental SAXS data. G) Model residuals H) Distribution of radii of gyration in the best 5-state models.

results confirmed that the N-terminal domain is an intrinsically disordered region in the RAD51 monomer as well as in the RAD51-BRC4 complex. Therefore, upon binding to the ATPase domain of a second RAD51 protomer, the N-terminal domain would assume a structured arrangement prone to fibril formation. By contrast, SAXS data on monomeric RAD51 and on RAD51-BRC4 complex indicate that, upon binding of the BRC repeats, a conformational change at the N-terminal domain is triggered leading to a rearrangement from a more ordered to a more disordered state. The detailed mechanism of RAD51 fibril disassembly was recently described as a multistep process, in which BRC4 erodes RAD51 fibrils from their termini through a "domino" mechanism.[13] This yields monomeric RAD51, which is the first essential step in BRCA2-mediated homologous recombination.[13] AF2 predicted a conformational shift of RAD51 N-terminal when it is in complex with BRC4 (Figure 7). This suggests that the LFDE domain of BRC4 could interact with RAD51 N-terminal domain, in agreement with previous publications,[26] thus rearranging it as an intrinsically disordered region, as shown by SAXS. Overall, these results suggest that in the disassembly of

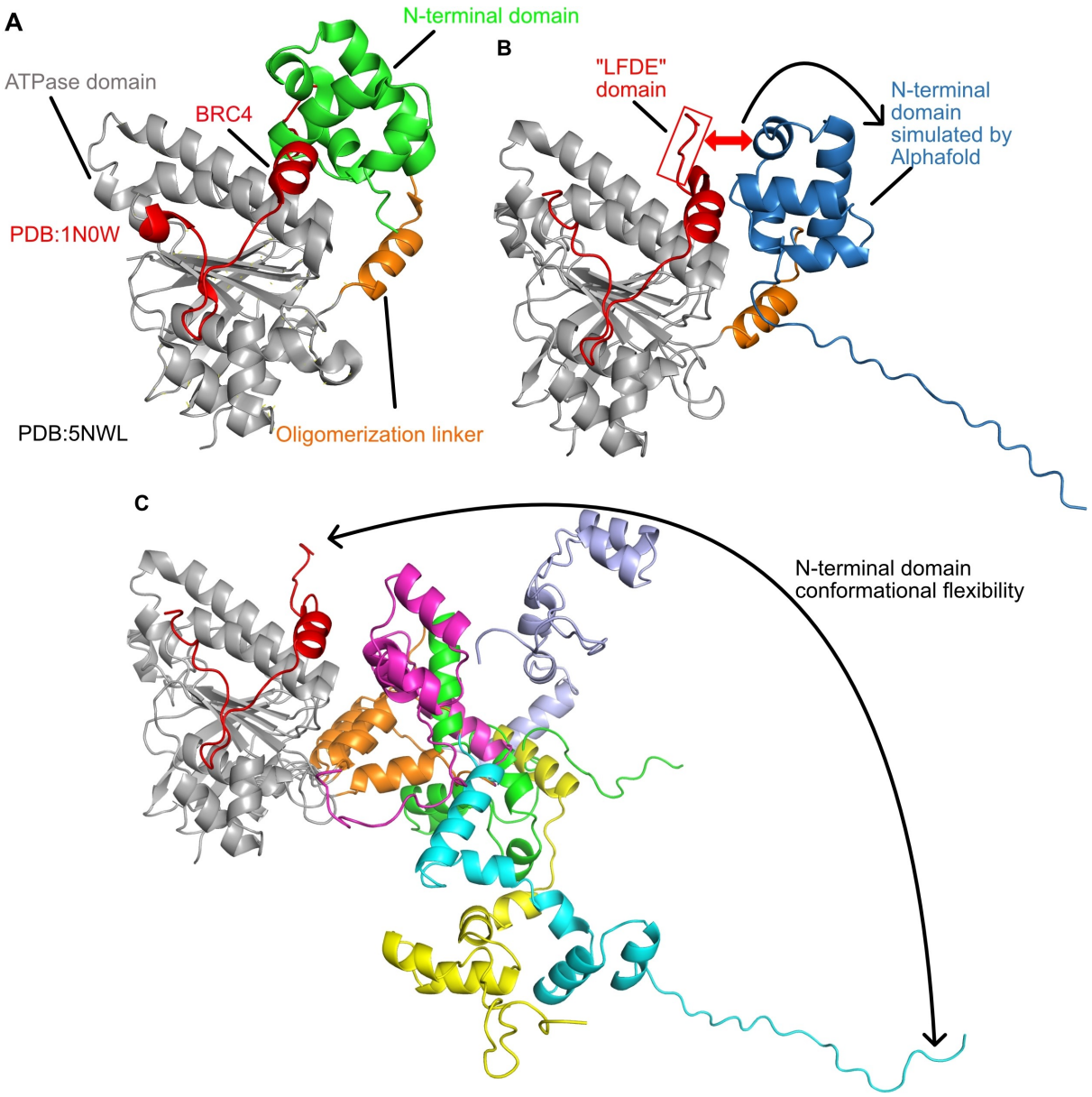

Figure 7. BRC4 and the RAD51 N-Terminal domain. A) Overlay of a RAD51 monomer (PDB entry: 5NWL) and the RAD51-BRC4 complex (PDB entry:1N0W). In grey is represented the ATPase domain, in orange the oligomerization linker and in green the N-terminal domain. The LFDE domain of BRC4 clashes with RAD51 N-terminal domain. B) The AF2 RAD51-BRC4 complex. In grey is represented the ATPase domain, in orange the oligomerization linker and in blue the N-terminal domain. In this case the N-terminal domain is shifted into another position and allows the binding of BRC4. C) Overlay of the 5-state Multi-FoXS models. Once the peptide has bound to RAD51, the N-terminal domain is free to move into solvent and can explore multiple conformations.

RAD51 fibrils operated by BRCA2 the unlocking of the N-terminal domain from the in fibril structured conformation to the disordered conformation is a critical step towards the formation of the monomeric RAD51 form suitable for recruitment and translocation into the nucleus at the site of DNA damage. Hence, the monomeric RAD51 reported here could be the most appropriate protein form for further investigating the critical steps during the early phases of the homologous recombination.

Conclusion

In this study, we have reported the isolation of a monomeric form of RAD51, a key player in homologous recombination and an emerging target for anticancer drug discovery within the synthetic lethality paradigm. In the past, mechanistic and drug discovery studies on this target, which has an inherent tendency to self- oligomerization, have significantly been hampered by the absence of a stable RAD51 monomeric form. In this work, the stability of a purified RAD51 protein harboring the mutation of two residues [F86E, A89E]

critical for RAD51 oligomerization has been investigated. Interestingly, we observed that these mutations, even though localized in the oligomerization linker of the protein, do not lead per se to a monomeric RAD51. Indeed, the protein still appears to retain the ability to form oligomeric structures, albeit with a different morphology. This observation agrees with recent studies on the single mutated [F86E] RAD51 and suggests a reduction of the protomer-protomer affinity.[22] Prompted by the presence of sulfate anions in the ATP binding site of the crystallized structures of RAD51 orthologues *Pf*RadA, *Sc*RAD51, we stabilized the monomeric form of the doubly mutated RAD51 by the addition of Na_2SO_4 to the buffer. To unravel the mechanism underlying the stabilization of the monomeric RAD51 form, we referred to a recent publication suggesting that conformational changes occur in RAD51 fibrils upon ATP hydrolysis to ADP.[47] Since sulfate anions may mimic the β-phosphates of ATP/ADP, we hypothesized that ADP and SO_4^{2-} may induce similar structural arrangements of RAD51. Hence, the effects of buffer containing ADP/Mg^{2+} or Na_2SO_4 were evaluated and compared. In line with previous biochemical studies,[29] our data support a possible competition of sulfate anions with the ATP for the same binding site. We also verified that the monomeric form of RAD51 binds BRC4 and CAM833A. SAXS studies on the monomeric RAD51 and the RAD51-BRC4 complex, coupled with modeling of the experimental data, suggest that the N-terminal domain of RAD51 is an intrinsically disordered region. Experimental data and AF2 predictions aimed at comparing monomeric RAD51 alone and in complex with BRC4 suggest that upon binding of BRC4 to RAD51 fibrils, the N-terminal domain shifts and rearranges into an intrinsically disordered region. This behavior provides a clear explanation for the difficulties met in obtaining a 3D structure of full-length RAD51 in complex with BRC4. We here propose the monomeric RAD51 as an innovative tool for conducting biophysical studies with partner interactors or with novel inhibitors of the BRCA2-RAD51 interaction with the ultimate goal to deepen the structural and mechanistic knowledge of the complex DNA repair system in which RAD51 plays a decisive role. The monomeric RAD51 form is a valuable tool for drug discovery investigations, as it not only provides a preserved RAD51-BRC4 binding site, as in the available chimeric RAD51 structures, but it also displays the overall human RAD51 3D structure thus allowing to examine additional binding sites, third-partner interactions or conformational rearrangements that are beyond the reach of chimeras. Given the flexibility of the N-terminal domain, future investigations will exploit alternative approaches to generate novel insights into the BRCA2-RAD51 interaction.

Acknowledgements

Francesco Rinaldi is the recipient of an AIRC Fellowship 2020 "Ignazia-La-Russa" Id.25239. This work was further supported by the Italian Association for Cancer Research (AIRC) through Grant IG 2018 Id.21386 awarded to Prof. Andrea Cavalli and the Istituto Italiano di Tecnologia (IIT). This work was partially supported by the Italian Ministry of Health with Ricerca Corrente and 5×1000 funds. The authors thank the B21 at Diamond Light Source (DLS) for providing the synchrotron radiation facility for SAXS measurements, and Giuseppe Ciossani, Francesca Rizzelli, Mattia Bernetti and Edoardo Gelardi for fruitful discussions.

Conflict of Interest

The authors declare no conflict of interest.

Data Availability Statement

The data that support the findings of this study are openly available in SASBDB at https://www.sasbdb.org/, reference number SASDQ97, SASDQT9, SASDQU9.

Keywords: DNA Damage · Protein Engineering · Protein-Protein Interactions · RAD51 · Structural Biology

[1] T. Lindahl, *Nature* **1993**, *362*, 709–15.
[2] S. C. West, *Nat. Rev. Mol. Cell Biol.* **2003**, *4*, 435–45.
[3] C. Stok, Y. P. Kok, N. van den Tempel, M. A. T. M. van Vugt, *Nucleic Acids Res.* **2021**, *49*, 4239–4257.
[4] I. Brouwer, T. Moschetti, A. Candelli, E. B. Garcin, M. Modesti, L. Pellegrini, G. J. Wuite, E. J. Peterman, *EMBO J.* **2018**, *37*, e98162.
[5] J. Xu, L. Zhao, Y. Xu, W. Zhao, P. Sung, H. W. Wang, *Nat. Struct. Mol. Biol.* **2017**, *24*, 40–46.
[6] J. M. Short, Y. Liu, S. Chen, N. Soni, M. S. Madhusudhan, M. K. K. Shivji, A. R. Venkitaraman, *Nucleic Acids Res.* **2016**, *44*, 9017–9030.
[7] F. Daboussi, A. Dumay, F. Delacôte, B. S. Lopez, *Cell. Signalling* **2002**, *14*, 969–75.
[8] W. K. Holloman, *Nat. Struct. Mol. Biol.* **2011**, *18*, 748–54.
[9] R. B. Jensen, A. Carreira, S. C. Kowalczykowski, *Nature* **2010**, *467*, 678–683.
[10] T. Shahid, J. Soroka, E. H. Kong, L. Malivert, M. J. McIlwraith, T. Pape, S. C. West, X. Zhang, *Nat. Struct. Mol. Biol.* **2014**, *21*, 962–968.
[11] L. Pellegrini, D. S. Yu, T. Lo, S. Anand, M. Y. Lee, T. L. Blundell, A. R. Venkitaraman, *Nature* **2002**, *420*, 287–293.
[12] J. Nomme, A. Renodon-Cornière, Y. Asanomi, K. Sakaguchi, A. Z. Stasiak, A. Stasiak, B. Norden, V. Tran, M. Takahashi, *J. Med. Chem.* **2010**, *53*, 5782–5791.
[13] F. Schipani, M. Manerba, R. Marotta, L. Poppi, A. Gennari, F. Rinaldi, A. Armirotti, F. Farabegoli, M. Roberti, G. Di Stefano, W. Rocchia, S. Girotto, N. Tirelli, A. Cavalli, *Int. J. Mol. Sci.* **2022**, *23*, 8338.
[14] D. E. Scott, M. Marsh, T. L. Blundell, C. Abell, M. Hyvönen, *FEBS Lett.* **2016**, *590*, 1094–1102.
[15] A. Carreira, S. C. Kowalczykowski, *Proc. Natl. Acad. Sci. USA* **2011**, *108*, 10448–53.
[16] S. H. Myers, J. A. Ortega, A. Cavalli, *J. Med. Chem.* **2020**, *63*, 14151–14183.
[17] G. Bagnolini, D. Milano, M. Manerba, F. Schipani, J. A. Ortega, D. Gioia, F. Falchi, A. Balboni, F. Farabegoli, F. De Franco, J. Robertson, R. Pellicciari, I. Pallavicini, S. Peri, S.

Minucci, S. Girotto, G. Di Stefano, M. Roberti, A. Cavalli, *J. Med. Chem.* **2020**, *63*, 2588–2619.
[18] F. Falchi, E. Giacomini, T. Masini, N. Boutard, L. Di Ianni, M. Manerba, F. Farabegoli, L. Rossini, J. Robertson, S. Minucci, I. Pallavicini, G. Di Stefano, M. Roberti, R. Pellicciari, A. Cavalli, *ACS Chem. Biol.* **2017**, *12*, 2491–2497.
[19] M. Roberti, F. Schipani, G. Bagnolini, D. Milano, E. Giacomini, F. Falchi, A. Balboni, M. Manerba, F. Farabegoli, F. De Franco, J. Robertson, S. Minucci, I. Pallavicini, G. Di Stefano, S. Girotto, R. Pellicciari, A. Cavalli, *Eur. J. Med. Chem.* **2019**, *165*, 80–92.
[20] D. E. Scott, N. J. Francis-Newton, M. E. Marsh, A. G. Coyne, G. Fischer, T. Moschetti, A. R. Bayly, T. D. Sharpe, K. T. Haas, L. Barber, C. R. Valenzano, R. Srinivasan, D. J. Huggins, M. Lee, A. Emery, B. Hardwick, M. Ehebauer, C. Dagostin, A. Esposito, L. Pellegrini, T. Perrior, G. McKenzie, T. L. Blundell, M. Hyvönen, J. Skidmore, A. R. Venkitaraman, C. Abell, *Cell Chem. Biol.* **2021**, *28*, 835–847.e5.
[21] T. Moschetti, T. Sharpe, G. Fischer, M. E. Marsh, H. K. Ng, M. Morgan, D. E. Scott, T. L. Blundell, A. R. Venkitaraman, J. Skidmore, C. Abell, M. Hyvönen, *J. Mol. Biol.* **2016**, *428*, 4589–4607.
[22] F. Paoletti, A. H. El-Sagheer, J. Allard, T. Brown, O. Dushek, F. Esashi, *EMBO J.* **2020**, *39*, e103002.
[23] M. M. Mundia, V. Desai, A. C. Magwood, M. D. Baker, *Genetics* **2014**, *197*, 107–119.
[24] L. H. Lindenburg, T. Pantelejevs, F. Gielen, P. Zuazua-Villar, M. Butz, E. Rees, C. F. Kaminski, J. A. Downs, M. Hyvönen, F. Hollfelder, *Proc. Natl. Acad. Sci. USA* **2021**, *118*, e2017708118.
[25] V. E. Galkin, F. Esashi, X. Yu, S. Yang, S. C. West, E. H. Egelman, *Proc. Natl. Acad. Sci. USA* **2005**, *102*, 8537–8542.
[26] S. Subramanyam, W. T. Jones, M. Spies, M. A. Spies, *Nucleic Acids Res.* **2013**, *41*, 9020–9032.
[27] D. J. Cole, E. Rajendra, M. Roberts-Thomson, B. Hardwick, G. J. McKenzie, M. C. Payne, A. R. Venkitaraman, C. K. Skylaris, *PLoS Comput. Biol.* **2011**, https://doi.org/10.1371/journal.pcbi.1002096.
[28] M. E. Marsh, D. E. Scott, M. T. Ehebauer, C. Abell, T. L. Blundell, M. Hyvönen, *FEBS Open Bio* **2016**, *6*, 372–85.
[29] K.-S. Shim, C. Schmutte, K. Yoder, R. Fishel, *DNA Repair* **2006**, *5*, 718–30.
[30] R. Amunugama, R. Fishel, *PLoS One* **2011**, *6*, e23071.
[31] D. S. Shin, *EMBO J.* **2003**, *22*, 4566–4576.
[32] A. B. Conway, T. W. Lynch, Y. Zhang, G. S. Fortin, C. W. Fung, L. S. Symington, P. A. Rice, *Nat. Struct. Mol. Biol.* **2004**, *11*, 791–6.
[33] A. Micsonai, É. Moussong, F. Wien, E. Boros, H. Vadászi, N. Murvai, Y.-H. Lee, T. Molnár, M. Réfrégiers, Y. Goto, Á. Tantos, J. Kardos, *Nucleic Acids Res.* **2022**, *50*, W90-W98.
[34] R. B. Robertson, D. N. Moses, Y. H. Kwon, P. Chan, P. Chi, H. Klein, P. Sung, E. C. Greene, *Proc. Natl. Acad. Sci. USA* **2009**, *106*, 12688–12693.
[35] A. M. Rossi, C. W. Taylor, *Nat. Protoc.* **2011**, *6*, 365–87.
[36] C. Dalvit, A. Parent, F. Vallée, M. Mathieu, A. Rak, *ChemMedChem* **2019**, *14*, 1115–1127.
[37] P. Bernadó, *Eur. Biophys. J.* **2010**, *39*, 769–780.
[38] D. Durand, C. Vivès, D. Cannella, J. Pérez, E. Pebay-Peyroula, P. Vachette, F. Fieschi, *J. Struct. Biol.* **2010**, *169*, 45–53.
[39] A. G. Kikhney, D. I. Svergun, *FEBS Lett.* **2015**, *589*, 2570–2577.
[40] H. Aihara, Y. Ito, H. Kurumizaka, S. Yokoyama, T. Shibata, *J. Mol. Biol.* **1999**, *290*, 495–504.
[41] D. Schneidman-Duhovny, M. Hammel, J. A. Tainer, A. Sali, *Biophys. J.* **2013**, *105*, 962–974.
[42] M. Mirdita, K. Schütze, Y. Moriwaki, L. Heo, S. Ovchinnikov, M. Steinegger, *Nat. Methods* **2022**, *19*, 679–682.
[43] J. Jumper, R. Evans, A. Pritzel, T. Green, M. Figurnov, O. Ronneberger, K. Tunyasuvunakool, R. Bates, A. Žídek, A. Potapenko, A. Bridgland, C. Meyer, S. A. A. Kohl, A. J. Ballard, A. Cowie, B. Romera-Paredes, S. Nikolov, R. Jain, J. Adler, T. Back, S. Petersen, D. Reiman, E. Clancy, M. Zielinski, M. Steinegger, M. Pacholska, T. Berghammer, S. Bodenstein, D. Silver, O. Vinyals, A. W. Senior, K. Kavukcuoglu, P. Kohli, D. Hassabis, *Nature* **2021**, *596*, 583–589.
[44] D. Schneidman-Duhovny, M. Hammel, J. A. Tainer, A. Sali, *Nucleic Acids Res.* **2016**, *44*, W424-W429.
[45] P. Bernadó, E. Mylonas, M. V. Petoukhov, M. Blackledge, D. I. Svergun, *J. Am. Chem. Soc.* **2007**, *129*, 5656–5664.
[46] G. Tria, H. D. T. Mertens, M. Kachala, D. I. Svergun, *IUCrJ* **2015**, *2*, 207–217.
[47] R. Appleby, D. Bollschweiler, D. Y. Chirgadze, L. Joudeh, L. Pellegrini, *iScience* **2023**, *26*, 106689.

Manuscript received: August 25, 2023
Accepted manuscript online: November 4, 2023
Version of record online: ■■, ■■

Research Articles

Biophysics

F. Rinaldi, F. Schipani, B. Balboni, F. Catalano, R. Marotta, S. H. Myers, V. Previtali, M. Veronesi, L. Scietti, V. Cecatiello, S. Pasqualato, J. A. Ortega, S. Girotto,* A. Cavalli* ____ **e202312517**

Isolation and Characterization of Monomeric Human RAD51: A Novel Tool for Investigating Homologous Recombination in Cancer

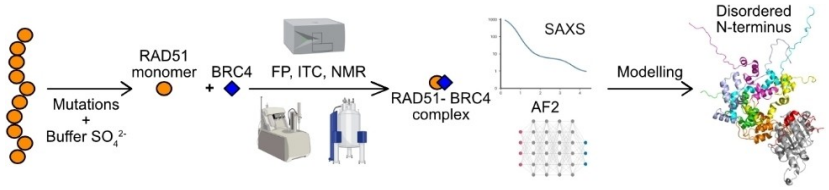

We report the isolation of a fully human monomeric RAD51, a unique tool for cancer research. Biophysical assays—isothermal titration calorimetry (ITC), fluorescence polarization (FP), and nuclear magnetic resonance (NMR)—allowed evaluating the ability of the protein to retain the binding to BRC4. AlphaFold2 (AF2) modeling of small-angle X-ray scattering (SAXS) data revealed novel insights on the RAD51 behavior upon BRC4 binding.